

Electron and hole spin relaxation in InP-based self-assembled quantum dots emitting at telecom wavelengths

A. V. Mikhailov,^{1,2} V. V. Belykh,^{1,3,*} D. R. Yakovlev,^{1,4} P. S. Grigoryev,^{1,2}
J. P. Reithmaier,⁵ M. Benyoucef,⁵ and M. Bayer^{1,4}

¹*Experimentelle Physik 2, Technische Universität Dortmund, D-44221 Dortmund, Germany*

²*Spin Optics Laboratory, St. Petersburg State University, 199034 St. Petersburg, Russia*

³*P.N. Lebedev Physical Institute of the Russian Academy of Sciences, 119991 Moscow, Russia*

⁴*Ioffe Institute, Russian Academy of Sciences, 194021 St. Petersburg, Russia*

⁵*Institute of Nanostructure Technologies and Analytics (INA), CINSA, University of Kassel, D-34132 Kassel, Germany*



(Received 26 June 2018; revised manuscript received 1 November 2018; published 26 November 2018)

We investigate the electron and hole spin relaxation in an ensemble of self-assembled InAs/In_{0.53}Al_{0.24}Ga_{0.23}As/InP quantum dots with emission wavelengths around 1.5 μm by using pump-probe Faraday rotation spectroscopy. Electron-spin dephasing due to the randomly oriented nuclear Overhauser fields is observed. At low temperatures we find a submicrosecond longitudinal electron-spin relaxation time T_1 which depends unexpectedly strongly on temperature. At high temperatures the electron-spin relaxation time is limited by optical phonon scattering through spin-orbit interaction decreasing down to 0.1 ns at 260 K. We show that the hole spin relaxation is activated much more effectively by a temperature increase compared with the electrons.

DOI: [10.1103/PhysRevB.98.205306](https://doi.org/10.1103/PhysRevB.98.205306)

I. INTRODUCTION

Semiconductor quantum dots (QDs) offer a promising platform for quantum information technologies [1]. An electron spin in a QD, often considered as a candidate for a quantum bit (qubit), can be efficiently manipulated by light pulses which gives the possibility of easy integration into existing optical telecommunication networks. In this respect QDs emitting in the telecom spectral range (1.3–1.6 μm) are especially attractive [2–12]. In particular, potential applications such as laser active media [6–8], single-photon emitters [13–21], and polarization-entangled photon emitters [22] are envisaged.

While for III-V QDs emitting in the technologically and spectroscopically easily accessible wavelength range below 1 μm the spin properties have been intensively studied in recent decades [23–34], information on the spin dynamics of QDs emitting at longer wavelengths, in particular in the telecom spectral range, is limited. So far, the electron and hole g factors [35] with record-high anisotropies [36–38] were measured. The dynamics of the photoluminescence polarization degree related to the exciton spin dynamics was measured as well [39].

In this paper we address the spin lifetimes of carriers in InAs/In_{0.53}Al_{0.24}Ga_{0.23}As/InP QDs emitting at telecom wavelengths, which have not been measured so far to the best of our knowledge. At weak magnetic fields, the spin dynamics of the resident electrons in the QDs is governed by the hyperfine interaction with the nuclei, and the regime described theoretically in Ref. [40] is observed. In increased longitudinal magnetic fields, at low temperatures we observe a submicrosecond decay of spin polarization. With increasing

temperature we observe a drastic decrease of both T_1 and T_2^* which at high temperatures is mediated by the electron interaction with LO phonons.

II. EXPERIMENTAL DETAILS

The QD sample was grown by molecular-beam epitaxy on an (100)-oriented InP substrate. The nominally undoped QDs were formed from 5.5 monolayers of InAs sandwiched between In_{0.53}Al_{0.24}Ga_{0.23}As barriers. The optically active QDs have a diameter of ~ 50 nm and a height of ~ 10 nm; their density is about 10^{10} cm^{-2} .

The sample is held at temperatures in the range 5–260 K in a helium bath cryostat with a split-coil superconducting magnet. Magnetic fields up to $B = 2$ T are applied either in Faraday (parallel to the light propagation direction, coinciding with the sample growth axis) or in Voigt (perpendicular to the light propagation direction) geometry. Pump-probe Faraday rotation is employed to study the carriers spin dynamics in the QDs [23]. Two laser systems are used. The first one consists of a mode-locked Yb:KGW laser pumping an optical parametric amplifier and has the pulse repetition frequency of 40 MHz (repetition period $T_R = 25$ ns). The second laser system is composed of a pulsed Ti:sapphire laser pumping an optical parametric oscillator (OPO) and has the pulse repetition rate of 76 MHz ($T_R = 13$ ns). The spectral width of the laser systems was shaped below 20 nm, centered at 1520 nm which matches the QD luminescence spectrum [35,36]. The pulse duration for both systems is less than 2 ps.

The laser beam is split into the pump and the probe. The pump pulses are circularly polarized and create carrier spin polarization in the QDs. The mechanism of optical spin orientation in QDs is described in Refs. [23,41]. The carriers' spin polarization is analyzed by measuring the Faraday

*vasilii.belykh@tu-dortmund.de

ellipticity of the initially linearly polarized probe pulses after transmission through the sample [42]. Varying the time delay between the pump and probe pulses by a mechanical delay line gives the time dependence of the spin polarization. The polarization of the pump beam is modulated between σ^+ and σ^- by a photo-elastic modulator for synchronous detection.

III. RESULTS AND DISCUSSION

Figure 1(a) shows the dynamics of the Faraday ellipticity signal for the magnetic field applied in Voigt (B_V) and Faraday (B_F) geometries. In the Voigt geometry the dynamics is composed of the sum of two decaying oscillatory functions, and the corresponding fit is shown by the green dashed line. The two oscillation components correspond to the electron and the hole spin precession with g factors $|g_e| = 1.7$ and $|g_h| = 0.7$, respectively. This attribution is based on the detailed

investigation of the anisotropies and energy dependencies of these g factors, as well as on theoretical calculations [35,36]. Note that the signal may be contributed by charged and neutral QDs. In the latter case, the exchange interaction between electron and hole will lead to a nonlinear magnetic-field dependence of the precession frequency [43] as well as zero-field spin beats and fast spin dephasing due to inhomogeneous fine-structure splitting [44]. Both effects are not observed in the experiment [35], indicating either an exchange interaction lower than $1 \mu\text{eV}$ or/and that charged QDs contribute to the signal (the most probable scenario). In both cases we observe uncoupled precessions of the electron and hole spins. The dephasing time T_2^* of each of the carrier spin polarizations at low temperatures is determined by the random nuclear Overhauser fields \mathbf{B}_N (which act on the carrier spins via the hyperfine interaction) if the external magnetic field B_V is smaller than B_N . At higher B_V , on the other hand, the time T_2^* is determined by the spread of the g -factors δg in the QD ensemble [23]:

$$1/T_2^* \approx |g|\mu_B B_N/\hbar, \quad B_V \lesssim B_N, \quad (1a)$$

$$1/T_2^* \approx \delta g \mu_B B_V/\hbar, \quad B_V \gg B_N. \quad (1b)$$

Therefore, as was shown for the same QDs in Refs. [35,36], an increase in B_V causes a decrease of the signal decay time.

In a longitudinal magnetic field B_F , the spin polarization decays monotonically without oscillations [36,45]. In sufficiently high B_F , this decay is characterized by a fast component with a decay time of 0.6 ns, close to the exciton lifetime, and a slow component of somewhat smaller amplitude. The existence of the long-living component indicates the presence of *resident* charge carriers in a fraction of the QD ensemble. The decay of the slow component is determined by the longitudinal spin relaxation time T_1 , which at low temperatures exceeds the period between the laser pulses T_R . This leads to an accumulation of spin polarization, and a signal offset appears at negative pump-probe delays, which can be identified in the Faraday geometry data in Fig. 1(a). Note that this offset is absent in the Voigt geometry.

The effects of longitudinal and transverse magnetic fields on the carrier spin polarization at a small negative delay $\Delta t = -0.15$ ns (which is equivalent to a large delay $t \approx T_R$ after the previous laser pulse) are presented in Fig. 1(b); see the black and red lines, respectively. When the longitudinal magnetic field is scanned, the signal has a minimum at $B_F = 0$ and develops then into a polarization recovery curve (PRC). At sufficiently high longitudinal magnetic field, the PRC signal is mainly determined by the longitudinal spin relaxation time T_1 .

At zero field the decay of the total spin polarization is governed by the nuclear fields. For an arbitrary QD the direction of the total nuclear Overhauser field \mathbf{B}_N acting on an electron (a hole) spin is random. The electron-spin component perpendicular to \mathbf{B}_N precesses around \mathbf{B}_N . When precessing, this spin component is averaged over all QDs, and it decays on a short timescale given by Eq. (1a). On the other hand, the electron-spin component along \mathbf{B}_N decays during the much longer time T_1 . Averaging over all QDs and, thus, over all directions of \mathbf{B}_N , shows that the nonprecessing component amounts to $1/3$

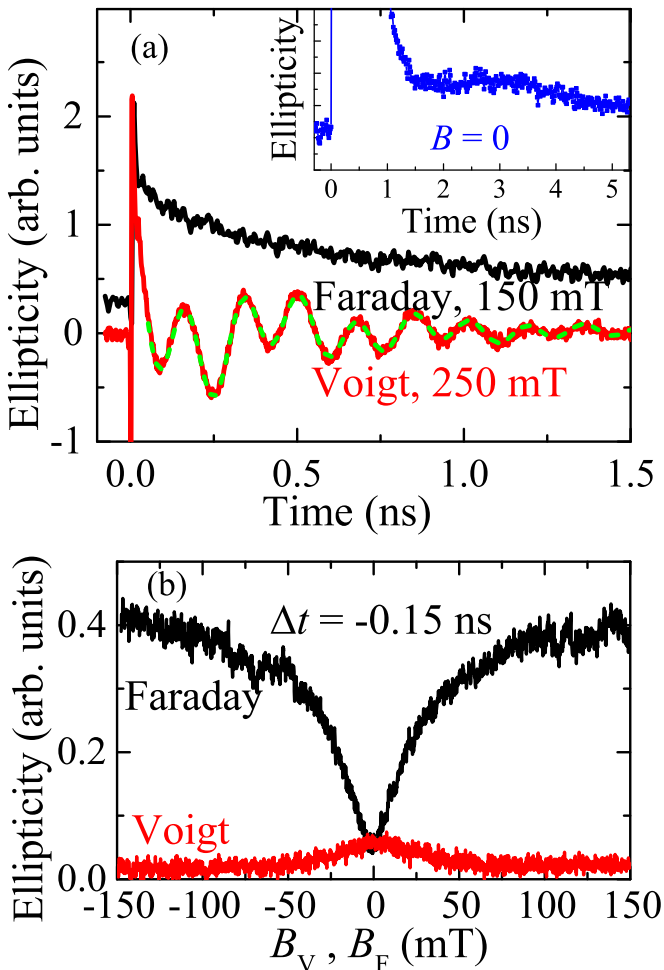


FIG. 1. (a) Dynamics of Faraday ellipticity signal for the magnetic field applied in Faraday (black line) and Voigt (red line) geometry, $T_R = 25$ ns. Green dashed line shows fit to the experimental data with two exponentially decaying oscillating functions. Inset shows dynamics at zero magnetic field with the focus on its non-monotonic behavior related to electron-spin precession in the nuclear Overhauser field. (b) Ellipticity signal as a function of magnetic field applied in Faraday (black line) and Voigt (red line) geometry at $t = -0.15$ ns, $T_R = 13$ ns. $T = 5$ – 10 K.

of the initial electron-spin polarization [32,33,40]. When the *longitudinal* magnetic field B_F is increased, the nonprecessing spin component along $\mathbf{B}_F + \mathbf{B}_N$ is increased, leading to an increase of the Faraday ellipticity signal due to accumulation of the long-living spin polarization. This simplified picture predicts the drop in the PRC curve [Fig. 1(b)] at $B_F = 0$ to $1/3$ from the signal at high B_F and the half width at half maximum (HWHM) of the PRC curve to be equal to B_N . However, a more detailed analysis should take into account the random nuclear-spin precession due to the quadrupole splitting which is especially large in the studied QDs having large strain. The effect of the nuclear-spin evolution on T_1 and on the shape of the PRC curve was considered in Ref. [41]. It was shown that a decreased correlation time τ_c of the nuclear-spin evolution, which for QDs typically is in the submicrosecond range, leads to (i) shortening of T_1 , (ii) an increase of the PRC drop-down amplitude, and (iii) an increase of the PRC width. We observe all three effects in the experiment. Indeed, (i) a decreased τ_c with respect to that in standard QDs emitting at shorter wavelengths results in a decreased T_1 [46], (ii) the spin polarization at $B_F = 0$ is less than $1/3$ of its value at high longitudinal magnetic fields (it amounts to only $\sim 1/8$), (iii) the nuclear field estimated from the electron T_2^* at zero external magnetic field using Eq. (1a) (11 mT) is less than the 30 mT HWHM of the PRC curve. A similar HWHM of the PRC curve was observed for negatively charged QDs emitting at shorter wavelength, while the corresponding HWHM for positively charged QDs is about 10 times smaller [46].

When the *transverse* magnetic field B_V is increased, it contributes to the nuclear field and the nonprecessing spin polarization (directed along $\mathbf{B}_V + \mathbf{B}_N$) has a vanishing projection on the probe beam direction. This leads to the decrease of the ellipticity signal at negative pump-probe delays with increasing B_V [Fig. 1(b), red line]. The half-width of the zero-field peak in this curve gives the value ≈ 30 mT, the same as in the PRC. Note that there are no resonant spin amplification [47] peaks at nonzero B_V due to the short transverse dephasing time T_2^* [see Eqs. (1a) and (1b)]. Another feature characteristic for an electron spin subject to nuclear fields is the nonmonotonic decay of the spin polarization in zero external magnetic field, showing a local minimum at the time of $(2 - 3)T_2^*$, where T_2^* can be estimated from Eq. (1a) [34,40]. This feature agrees with our observations at $t \approx 1.8$ ns [see the inset in Fig. 1(a)], despite the small amplitude of the minimum.

Next, we concentrate on evaluating the longitudinal spin relaxation time T_1 and studying its temperature dependence. At low temperatures we use the spin inertia method [48] for that purpose. To perform synchronous detection in these experiments, the intensity of the circularly polarized pump is modulated at frequency f : $P = P_0[1 + \cos(2\pi ft)]/2$. When the modulation period $1/f$ exceeds the T_1 time, the accumulated spin polarization is modulated from 0 up to the maximal value determined by the pumping rate P_0 and T_1 . When the modulation frequency is increased, so that $1/f$ becomes comparable to T_1 , the spin polarization decreases. One can show that, in the case $T_1 \gg T_R$, $1/f \gg T_R$, the accumulated spin polarization is given by

$$S(t) = P_0 T_1 + A \cos(2\pi ft - \phi), \quad (2)$$

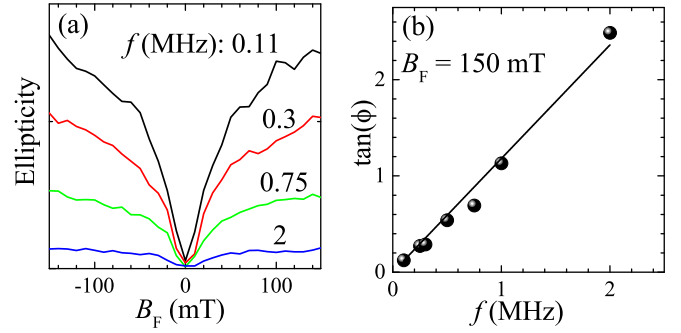


FIG. 2. Spin inertia effect. (a) Polarization recovery curves taken at a small negative delay for different pump modulation frequencies. The curves are vertically shifted to the same value at $B_F = 0$. (b) Frequency dependence of $\tan(\phi)$, where ϕ is the retardation phase of the spin-polarization modulation with respect to the pump modulation at $B_F = 150$ mT. The line shows a linear fit. $T = 5$ K, $T_R = 13$ ns.

$$A = \frac{P_0 T_1}{\sqrt{1 + (2\pi T_1 f)^2}}, \quad (3)$$

$$\tan(\phi) = 2\pi T_1 f. \quad (4)$$

Thus, with increasing f , the modulation of the spin polarization decreases in amplitude A [Eq. (3)] and becomes retarded relative to the pump modulation by the phase ϕ [Eq. (4)]. By performing synchronous detection on the pumping frequency f , we are able to measure both A and ϕ . Figure 2(a) shows PRCs measured at different pump modulation frequencies. The ellipticity, reflecting the amplitude of the spin polarization, instead decreases with increasing f . Figure 2(b) shows that $\tan(\phi)$ increases almost linearly with f , in agreement with Eq. (4), allowing us to estimate $T_1 \approx 190$ ns from Eq. (4) at $B_F = 150$ mT.

Let us make two remarks about the spin inertia method and the validity of Eqs. (2)–(4). First, we do not take into account the saturation effect in QDs: at sufficiently high pump powers and sufficiently long T_1 , the majority of QDs becomes spin-polarized and is no longer affected by further pumping. A more detailed analysis shows that the saturation leads to an effective shortening of T_1 entering into Eqs. (2)–(4). Second, the above analysis assumes a monoexponential dynamics of the spin polarization, characterized by a single time T_1 . One can show that, in the case of a more complex dynamics, the dependence of the spin-polarization modulation amplitude on f [Eq. (3)] is dominated by the slow component, while the frequency dependence of the retardation phase ϕ [Eq. (4)] is dominated by the fast component. Thus, the estimated value $T_1 = 190$ ns is the lower limit for the decay time of the fast component in the longitudinal spin-polarization dynamics.

The temperature dependence of the longitudinal spin relaxation time T_1 is shown in Fig. 3 by stars. At $T \leq 10$ K, the times T_1 are determined by the spin inertia method. For $15 \leq T \leq 50$ K, where T_1 becomes comparable to the laser repetition period T_R , they are extracted from the ratio of the ellipticity signals in the PRC curves at different time delays $S(t + \Delta t)/S(t) = \exp(-\Delta t/T_1)$ (see inset in Fig. 3). Note

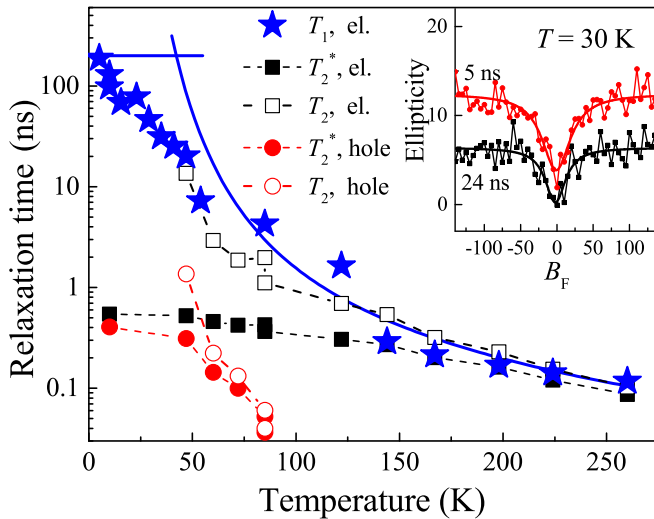


FIG. 3. Temperature dependencies of longitudinal electron-spin relaxation time T_1 (stars), inhomogeneous transverse spin relaxation times T_2^* for electrons and holes (solid squares and circles, respectively), and homogeneous transverse spin relaxation times T_2 for electrons and holes (open squares and circles, respectively). Solid lines show zero-temperature value of T_1 and T_1 determined by relaxation with LO phonons according to Eq. (6). Dashed lines are to guide the eye. Inset shows polarization recovery curves measured at different time delays (symbols) fit with Lorentzians (solid lines) at $T = 30$ K.

that this ratio weakly depends on $|B_F| < 150$ mT, and for final T_1 determination we took the ratio of the PRC dip depths. For higher temperatures ($T > 50$ K), where $T_1 < T_R$, T_1 was directly determined as the decay time of the slow component of the ellipticity signal at $B_F = 150$ mT.

It is instructive to compare the temperature dependence of T_1 to that of T_2^* for electrons and holes (see Fig. 3, solid squares and circles, respectively). The times T_2^* for electrons and holes are determined from the decay of two oscillating components in the transverse magnetic field $B_V = 250$ mT [see Fig. 1(a)]. At low temperatures T_2^* is determined by the nuclear field and the spread of g factors [Eqs. (1a) and (1b)] and is much shorter than T_1 . At higher temperatures the homogeneous dephasing mechanisms related to phonons become important and T_2^* decreases with T . One can separate the inhomogeneous (T_2^{inh}) and homogeneous (T_2) contributions to T_2^* :

$$1/T_2^* = 1/T_2^{\text{inh}} + 1/T_2. \quad (5)$$

Note that T_2^{inh} is almost temperature independent as evidenced from the temperature-independent width of the PRC minimum (for $T < 50$ K where it can be measured) which is determined by the nuclear fields and from the temperature-independent spread of g factors, which is determined by the QD shape and composition spread. Taking into account that $T_2^{\text{inh}} \approx T_2^*(T = 0)$, we can estimate the homogeneous transverse spin relaxation times T_2 at elevated temperatures by using Eq. (5) (at least the part of the homogeneous spin relaxation rate that is temperature dependent). They are shown by the open squares and circles in Fig. 3 for electrons and holes, respectively. The decrease of T_2 with increasing tem-

perature is especially pronounced for holes. For electrons, T_2 is close to T_1 in the whole temperature range, as was predicted theoretically [49], which allows us to attribute the T_1 dependence and, in general, the long-living spin-polarization component to electrons that are resident in a fraction of QDs.

Now we discuss the origin of the T_1 temperature dependence for the electrons. In the limit of zero temperature, T_1 is determined by the hyperfine interaction with nuclear spins, as already discussed (horizontal solid line in Fig. 3). For sufficiently high temperatures, $T \gtrsim 50$ K, the spin relaxation is governed by the interaction with LO phonons [30,50,51]. In particular, the two-phonon mechanism with absorption and emission of an optical phonon leads to spin relaxation. The relaxation rate due to this process can be described by the following equation [30,50]:

$$1/T_{1,\text{LO}} = \beta N_{\text{LO}}(N_{\text{LO}} + 1), \quad (6)$$

$$N_{\text{LO}} = [\exp(\epsilon_{\text{LO}}/k_B T) - 1]^{-1},$$

where N_{LO} is the number of phonons, ϵ_{LO} is the LO phonon energy, and β defines the strength of the electron-phonon interaction. The corresponding dependence shown in Fig. 3 by the solid line with $\epsilon_{\text{LO}} = 30$ meV (LO phonon energy in InAs) and $\beta = 20$ ns $^{-1}$ fits the experimental data at high temperatures.

The relatively strong temperature dependence of T_1 for low temperatures, $T \lesssim 50$ K, is unclear. The usual temperature-dependent QD spin-relaxation mechanisms, spin-orbit interaction involving phonons [52], and phonon-activated electron-nuclear flip-flop processes [52–54], give rates several orders smaller than in the experiment. We note that, for the QDs emitting around 900 nm, a similar temperature dependence of T_2 was reported [28]. However, in that case the T_2 variation starts from $T = 15$ K, while in our case T_1 strongly depends on T already from 5 K. One possible source of temperature-dependent spin relaxation at low temperatures might be an exchange interaction with carriers in the wetting layer that are localized by shallow inhomogeneities. With a moderate increase of temperature these carriers become delocalized, activating the exchange interaction.

IV. CONCLUSION

To summarize, we have studied the longitudinal and transverse electron-spin relaxation in an ensemble of InAs/In $_{0.53}$ Al $_{0.24}$ Ga $_{0.23}$ As/InP quantum dots emitting in the telecom wavelength range. At weak magnetic fields, the major fraction of the total spin polarization decays on the nanosecond timescale due to precession of the individual spins in random nuclear fields. At increased longitudinal magnetic field the spin polarization decays during the submicrosecond time T_1 at low temperatures, which decreases by three orders of magnitude when approaching room temperature. At low temperatures ($T \lesssim 50$ K) we found a relatively strong variation of T_1 with T which is so far not understood, while at elevated temperatures ($T \gtrsim 50$ K) T_1 is dominated by spin-orbit relaxation with emission and absorption of an optical phonon. The transverse spin relaxation time T_2 at elevated temperatures is limited by the T_1 time.

ACKNOWLEDGMENTS

We are grateful to I. A. Yugova and N. E. Kopteva for useful discussions, to E. Kirstein for help with experiments, and to M. Yacob for help with the sample growth. Financial support from the Russian Foundation for Basic Research (RFBR, Project No. 15-52-12019) and Deutsche Forschungsgemeinschaft (DFG, Project A1) in the framework of International Collaborative Research Center TRR 160 is acknowledged. The Dortmund and Kassel teams acknowledge the support of

the BMBF in the frame of the Project Q.com-H (Contracts No. 16KIS0104K and No. 16KIS0112). The Dortmund team also acknowledges support by the BMBF-project Q.Link.X (Contract No. 16KIS0857). M.B. thanks the Ministry of Education and Science of the Russian Federation (Contract No. 14.Z50.31.0021). A.V.M. acknowledges Saint-Petersburg State University for the research grant 11.34.2.2012. P.S.G. acknowledges support by the Russian Foundation for Basic Research (RFBR, Project No. 18-32-00568).

-
- [1] D. Loss and D. P. DiVincenzo, Quantum computation with quantum dots, *Phys. Rev. A* **57**, 120 (1998).
- [2] S. Fafard, Z. Wasilewski, J. McCaffrey, S. Raymond, and S. Charbonneau, InAs self-assembled quantum dots on InP by molecular beam epitaxy, *Appl. Phys. Lett.* **68**, 991 (1996).
- [3] A. Ponchet, A. Le Corre, H. L'Haridon, B. Lambert, and S. Salaün, Relationship between self-organization and size of InAs islands on InP(001) grown by gas-source molecular beam epitaxy, *Appl. Phys. Lett.* **67**, 1850 (1995).
- [4] M. Taskinen, M. Sopanen, H. Lipsanen, J. Tulkki, T. Tuomi, and J. Ahopelto, Self-organized InAs islands on (100) InP by metalorganic vapor-phase epitaxy, *Surf. Sci.* **376**, 60 (1997).
- [5] C. Paranthoen, N. Bertru, O. Dehaese, A. Le Corre, S. Loualiche, B. Lambert, and G. Patriarche, Height dispersion control of InAs/InP quantum dots emitting at 1.55 μm , *Appl. Phys. Lett.* **78**, 1751 (2001).
- [6] H. Saito, K. Nishi, and S. Sugou, Ground-state lasing at room temperature in long-wavelength InAs quantum-dot lasers on InP(311)B substrates, *Appl. Phys. Lett.* **78**, 267 (2001).
- [7] R. H. Wang, A. Stintz, P. M. Varangis, T. C. Newell, H. Li, K. J. Malloy, and L. F. Lester, Room-temperature operation of InAs quantum-dot lasers on InP [001], *IEEE Photonics Technol. Lett.* **13**, 767 (2001).
- [8] F. Lelarge, B. Rousseau, B. Dagens, F. Poingt, F. Pommereau, and A. Accard, Room temperature continuous-wave operation of buried ridge stripe lasers using InAs-InP (100) quantum dots as active core, *IEEE Photonics Technol. Lett.* **17**, 1369 (2005).
- [9] P. J. van Veldhoven, N. Chauvin, A. Fiore, and R. Nötzel, Low density 1.55 μm InAs/InGaAsP/InP (100) quantum dots enabled by an ultrathin GaAs interlayer, *Appl. Phys. Lett.* **95**, 113110 (2009).
- [10] S.-K. Liao, H.-L. Yong, C. Liu, G.-L. Shentu, D.-D. Li, J. Lin, H. Dai, S.-Q. Zhao, B. Li, J.-Y. Guan, W. Chen, Y.-H. Gong, Y. Li, Z.-H. Lin, G.-S. Pan, J. S. Pelc, M. M. Fejer, W.-Z. Zhang, W.-Y. Liu, J. Yin, J.-G. Ren, X.-B. Wang, Q. Zhang, C.-Z. Peng, and J.-W. Pan, Long-distance free-space quantum key distribution in daylight towards inter-satellite communication, *Nat. Photonics* **11**, 509 (2017).
- [11] L. Sapienza, R. Al-Khuzeyri, A. Dada, A. Griffiths, E. Clarke, and B. D. Gerardot, Magneto-optical spectroscopy of single charge-tunable InAs/GaAs quantum dots emitting at telecom wavelengths, *Phys. Rev. B* **93**, 155301 (2016).
- [12] P. Mrowinski, M. Zielinski, M. Swiderski, J. Misiewicz, A. Somers, J. P. Reithmaier, S. Höfling, and G. Sek, Excitonic fine structure and binding energies of excitonic complexes in single InAs quantum dashes, *Phys. Rev. B* **94**, 115434 (2016).
- [13] T. Miyazawa, K. Takemoto, Y. Sakuma, S. Hirose, T. Usuki, N. Yokoyama, M. Takatsu, and Y. Arakawa, Single-photon generation in the 1.55- μm optical-fiber band from an InAs/InP quantum dot, *Jpn. J. Appl. Phys.* **44**, L620 (2005).
- [14] K. Takemoto, M. Takatsu, S. Hirose, N. Yokoyama, Y. Sakuma, T. Usuki, T. Miyazawa, and Y. Arakawa, An optical horn structure for single-photon source using quantum dots at telecommunication wavelength, *J. Appl. Phys.* **101**, 081720 (2007).
- [15] K. Takemoto, Y. Nambu, T. Miyazawa, K. Wakui, S. Hirose, T. Usuki, M. Takatsu, N. Yokoyama, K. Yoshino, A. Tomita, S. Yorozu, Y. Sakuma, and Y. Arakawa, Transmission experiment of quantum keys over 50 km using high-performance quantum-dot single-photon source at 1.5 μm wavelength, *Appl. Phys. Express* **3**, 092802 (2010).
- [16] M. D. Birowosuto, H. Sumikura, S. Matsuo, H. Taniyama, P. J. van Veldhoven, R. Nötzel, and M. Notomi, Fast Purcell-enhanced single photon source in 1,550-nm telecom band from a resonant quantum dot-cavity coupling, *Sci. Rep.* **2**, 321 (2012).
- [17] M. Benyoucef, M. Yacob, J. P. Reithmaier, J. Kettler, and P. Michler, Telecom-wavelength (1.5 μm) single-photon emission from InP-based quantum dots, *Appl. Phys. Lett.* **103**, 162101 (2013).
- [18] X. Liu, K. Akahane, N. A. Jahan, N. Kobayashi, M. Sasaki, H. Kumano, and I. Suemune, Single-photon emission in telecommunication band from an InAs quantum dot grown on InP with molecular-beam epitaxy, *Appl. Phys. Lett.* **103**, 061114 (2013).
- [19] L. Dusanowski, M. Syperek, P. Mrowinski, W. Rudno-Rudziński, J. Misiewicz, A. Somers, S. Höfling, M. Kamp, J. P. Reithmaier, and G. Sek, Single photon emission at 1.55 μm from charged and neutral exciton confined in a single quantum dash, *Appl. Phys. Lett.* **105**, 021909 (2014).
- [20] J.-H. Kim, T. Cai, C. J. K. Richardson, R. P. Leavitt, and E. Waks, Two-photon interference from a bright single-photon source at telecom wavelengths, *Optica* **3**, 577 (2016).
- [21] M. Paul, F. Olbrich, J. Höschele, S. Schreier, J. Kettler, S. L. Portalupi, M. Jetter, and P. Michler, Single-photon emission at 1.55 μm from MOVPE-grown InAs quantum dots on InGaAs/GaAs metamorphic buffers, *Appl. Phys. Lett.* **111**, 033102 (2017).
- [22] F. Olbrich, J. Höschele, M. Müller, J. Kettler, S. L. Portalupi, M. Paul, M. Jetter, and P. Michler, Polarization-entangled photons from an InGaAs-based quantum dot emitting in the telecom C-band, *Appl. Phys. Lett.* **111**, 133106 (2017).
- [23] D. R. Yakovlev and M. Bayer, Coherent spin dynamics of carriers, in *Spin Physics in Semiconductors*, edited by M. I.

- Dyakonov, Springer Series in Solid-State Sciences Vol. 157 (Springer International Publishing, Cham, Switzerland, 2017), p. 155.
- [24] M. Bayer, A. Kuther, A. Forchel, A. Gorbunov, V. B. Timofeev, F. Schäfer, J. P. Reithmaier, T. L. Reinecke, and S. N. Walck, Electron and Hole g Factors and Exchange Interaction from Studies of the Exciton Fine Structure in $\text{In}_{0.60}\text{Ga}_{0.40}\text{As}$ Quantum Dots, *Phys. Rev. Lett.* **82**, 1748 (1999).
- [25] M. Kroutvar, Y. Ducommun, D. Heiss, M. Bichler, D. Schuh, G. Abstreiter, and J. J. Finley, Optically programmable electron spin memory using semiconductor quantum dots, *Nature (London)* **432**, 81 (2004).
- [26] M. V. Gurudev Dutt, J. Cheng, B. Li, X. Xu, X. Li, P. R. Berman, D. G. Steel, A. S. Bracker, D. Gammon, S. E. Economou, R. B. Liu, and L. J. Sham, Stimulated and Spontaneous Optical Generation of Electron Spin Coherence in Charged GaAs Quantum Dots, *Phys. Rev. Lett.* **94**, 227403 (2005).
- [27] A. Greilich, R. Oulton, E. A. Zhukov, I. A. Yugova, D. R. Yakovlev, M. Bayer, A. Shabaev, Al L. Efros, I. A. Merkulov, V. Stavarache, D. Reuter, and A. Wieck, Optical Control of Spin Coherence in Singly Charged (In,Ga)As/GaAs Quantum Dots, *Phys. Rev. Lett.* **96**, 227401 (2006).
- [28] F. G. G. Hernandez, A. Greilich, F. Brito, M. Wiemann, D. R. Yakovlev, D. Reuter, A. D. Wieck, and M. Bayer, Temperature-induced spin-coherence dissipation in quantum dots, *Phys. Rev. B* **78**, 041303 (2008).
- [29] F. Fras, B. Eble, P. Desfonds, F. Bernardot, C. Testelin, M. Chamarro, A. Miard, and A. Lemaître, Two-phonon process and hyperfine interaction limiting slow hole-spin relaxation time in InAs/GaAs quantum dots, *Phys. Rev. B* **86**, 045306 (2012).
- [30] X. M. Dou, B. Q. Sun, D. S. Jiang, H. Q. Ni, and Z. C. Niu, Temperature dependence of electron-spin relaxation in a single InAs quantum dot at zero applied magnetic field, *J. Appl. Phys.* **111**, 053524 (2012).
- [31] Y. G. Semenov and K. W. Kim, Elastic spin-relaxation processes in semiconductor quantum dots, *Phys. Rev. B* **75**, 195342 (2007).
- [32] P.-F. Braun, X. Marie, L. Lombez, B. Urbaszek, T. Amand, P. Renucci, V. K. Kalevich, K. V. Kavokin, O. Krebs, P. Voisin, and Y. Masumoto, Direct Observation of the Electron Spin Relaxation Induced by Nuclei in Quantum Dots, *Phys. Rev. Lett.* **94**, 116601 (2005).
- [33] B. Eble, C. Testelin, P. Desfonds, F. Bernardot, A. Balocchi, T. Amand, A. Miard, A. Lemaître, X. Marie, and M. Chamarro, Hole-Nuclear Spin Interaction in Quantum Dots, *Phys. Rev. Lett.* **102**, 146601 (2009).
- [34] A. Bechtold, D. Rauch, F. Li, T. Simmet, P.-L. Ardelit, A. Regler, Kai Müller, N. A. Sinitsyn, and J. J. Finley, Three-stage decoherence dynamics of an electron spin qubit in an optically active quantum dot, *Nat. Phys.* **11**, 1005 (2015).
- [35] V. V. Belykh, A. Greilich, D. R. Yakovlev, M. Yacob, J. P. Reithmaier, M. Benyoucef, and M. Bayer, Electron and hole g factors in InAs/InAlGaAs self-assembled quantum dots emitting at telecom wavelengths, *Phys. Rev. B* **92**, 165307 (2015).
- [36] V. V. Belykh, D. R. Yakovlev, J. J. Schindler, E. A. Zhukov, M. A. Semina, M. Yacob, J. P. Reithmaier, M. Benyoucef, and M. Bayer, Large anisotropy of electron and hole g factors in infrared-emitting InAs/InAlGaAs self-assembled quantum dots, *Phys. Rev. B* **93**, 125302 (2016).
- [37] J. van Bree, A. Yu. Silov, M. L. van Maasakkers, C. E. Pryor, M. E. Flatté, and P. M. Koenraad, Anisotropy of electron and hole g tensors of quantum dots: An intuitive picture based on spin-correlated orbital currents, *Phys. Rev. B* **93**, 035311 (2016).
- [38] V. V. Belykh, D. R. Yakovlev, J. J. Schindler, J. van Bree, P. M. Koenraad, N. S. Averkiev, M. Bayer, and A. Yu. Silov, Dispersion of the electron g factor anisotropy in InAs/InP self-assembled quantum dots, *J. Appl. Phys.* **120**, 084301 (2016).
- [39] M. Spereck, L. Dusanowski, M. Gawelczyk, G. Sęk, A. Somers, J. P. Reithmaier, S. Höfling, and J. Misiewicz, Exciton spin relaxation in InAs/InGaAlAs/InP(001) quantum dashes emitting near 1.55 μm , *Appl. Phys. Lett.* **109**, 193108 (2016).
- [40] I. A. Merkulov, Al. L. Efros, and M. Rosen, Electron spin relaxation by nuclei in semiconductor quantum dots, *Phys. Rev. B* **65**, 205309 (2002).
- [41] D. S. Smirnov, E. A. Zhukov, E. Kirstein, D. R. Yakovlev, D. Reuter, A. D. Wieck, M. Bayer, A. Greilich, and M. M. Glazov, Theory of spin inertia in singly charged quantum dots, *Phys. Rev. B* **98**, 125306 (2018).
- [42] I. A. Yugova, M. M. Glazov, E. L. Ivchenko, and Al. L. Efros, Pump-probe Faraday rotation and ellipticity in an ensemble of singly charged quantum dots, *Phys. Rev. B* **80**, 104436 (2009).
- [43] I. A. Yugova, A. Greilich, E. A. Zhukov, D. R. Yakovlev, M. Bayer, D. Reuter, and A. D. Wieck, Exciton fine structure in InGaAs/GaAs quantum dots revisited by pump-probe Faraday rotation, *Phys. Rev. B* **75**, 195325 (2007).
- [44] A. I. Tartakovskii, M. N. Makhonin, I. R. Sellers, J. Cahill, A. D. Andreev, D. M. Whittaker, J.-P. R. Wells, A. M. Fox, D. J. Mowbray, M. S. Skolnick, K. M. Groom, M. J. Steer, H. Y. Liu, and M. Hopkinson, Effect of thermal annealing and strain engineering on the fine structure of quantum dot excitons, *Phys. Rev. B* **70**, 193303 (2004).
- [45] V. V. Belykh, E. Evers, D. R. Yakovlev, F. Fobbe, A. Greilich, and M. Bayer, Extended pump-probe Faraday rotation spectroscopy of the submicrosecond electron spin dynamics in n -type GaAs, *Phys. Rev. B* **94**, 241202(R) (2016).
- [46] E. A. Zhukov, E. Kirstein, D. S. Smirnov, D. R. Yakovlev, M. M. Glazov, D. Reuter, A. D. Wieck, M. Bayer, and A. Greilich, Spin inertia of resident and photoexcited carriers in singly charged quantum dots, *Phys. Rev. B* **98**, 121304 (2018).
- [47] J. M. Kikkawa and D. D. Awschalom, Resonant Spin Amplification in n -Type GaAs, *Phys. Rev. Lett.* **80**, 4313 (1998).
- [48] F. Heisterkamp, E. A. Zhukov, A. Greilich, D. R. Yakovlev, V. L. Korenev, A. Pawlis, and M. Bayer, Longitudinal and transverse spin dynamics of donor-bound electrons in fluorine-doped ZnSe: Spin inertia versus Hanle effect, *Phys. Rev. B* **91**, 235432 (2015).
- [49] V. N. Golovach, A. Khaetskii, and D. Loss, Phonon-Induced Decay of the Electron Spin in Quantum Dots, *Phys. Rev. Lett.* **93**, 016601 (2004).
- [50] E. Tsitsishvili, R. V. Baltz, and H. Kalt, Temperature dependence of polarization relaxation in semiconductor quantum dots, *Phys. Rev. B* **66**, 161405 (2002).

- [51] T. Flissikowski, I. A. Akimov, A. Hundt, and F. Henneberger, Single-hole spin relaxation in a quantum dot, *Phys. Rev. B* **68**, 161309 (2003).
- [52] A. V. Khaetskii and Y. V. Nazarov, Spin-flip transitions between Zeeman sublevels in semiconductor quantum dots, *Phys. Rev. B* **64**, 125316 (2001).
- [53] S. I. Erlingsson, Y. V. Nazarov, and V. I. Fal'ko, Nucleus-mediated spin-flip transitions in GaAs quantum dots, *Phys. Rev. B* **64**, 195306 (2001).
- [54] V. A. Abalmassov and F. Marquardt, Electron-nuclei spin relaxation through phonon-assisted hyperfine interaction in a quantum dot, *Phys. Rev. B* **70**, 075313 (2004).